Analysis of Radar Return from Turbulent High-Altitude Rocket Exhaust Plumes

JAMES STARK DRAPER* AND PHILIP ONNI JARVINEN†
MITHRAS Division of Sanders Associates, Cambridge, Mass.

AND

THOMAS D. CONLEY‡
Air Force Cambridge Research Laboratories, Bedford, Mass.

An approximate analysis of radar backscattering from the underdense turbulent rocket exhaust plume at high altitudes is offered. The tail aspect radar backscatter spectral content is analyzed using an exhaust mean flow model that has been shown accurate for engineering analyses and upon which a gaussian velocity turbulence perturbation is superimposed. The turbulence intensity is directly related to combustion chamber temperature-fluctuations for small perturbations. The radar wave is assumed scattered from an elemental volume in the exhaust flow in which the turbulence is assumed quasi-isotropic and for which the flow properties vary negligibly over a radar wavelength. The resulting expressions yield the total and spectral radar cross section of the underdense plume backscattering in terms of engine combustion chamber temperature, temperature fluctuations, electron density, area ratio, throat diameter, exhaust gas ratio of specific heats, vehicle velocity and radar wavelength. Comparisons with data are made; however, little data is available and many aspects of the approximate theory offered cannot be confirmed at present.

Nomenclature

A_e = nozzle exit area
B = exhaust centerline decay parameter
c = speed of light
C_F = thrust coefficient
$C_{F\max}$ = maximum vacuum thrust coefficient
D = $2f_o\bar{V}_L/c\lambda_\infty$
d_e = engine exit diameter
f_o = radar frequency
f_p = plasma frequency
f_c = center frequency for return from hollow cone at θ
$f_{\max}$ = $f_o[1 + 2(\bar{V}_L - V_R)/c]$
k = $2\pi/\lambda_0$
l = turbulence correlation length
L = plume scale
M = Mach number
m = mass flow
n = electron density
$\overline{\Delta n^2}$ = mean square electron density turbulence
R = correlation function
r = radial distance from exit plane
r_o = exhaust location of overdense region limit
R_o = $4k^2r_o^2$ on centerline ($\theta = 0$)
s = scattering volume separation
T = gas temperature
u = velocity perturbation from $\bar{V}_L$
V_L = gas limiting velocity
V_R = rocket velocity
χ = incident field angle with scattering plane
X = normalized Doppler frequency
γ = gas specific heat
n_1 = index of refraction
η = $1 - \cos\theta$
θ = temperature perturbation; polar angle from exhaust centerline
λ_∞ = exhaust spreading parameter (see Sec. 2.1)
λ_o = freespace radar wavelength
ρ = gas density
σ = radar cross section
σ_T = Thompson cross section
σ_u = exhaust underdense cross section
σ_V = underdense vacuum exhaust cross section
τ = $X_c - X$
ϕ = scattering angle
Ω = solid angle
$(\ )^*$ = throat parameter
$(\bar{\ })$ = time average
$(\ )_c$ = chamber condition

Presented as Paper 69–71 at the AIAA 7th Aerospace Sciences Meeting, New York, January 20–22, 1969; submitted February 11, 1969; revision received February 18, 1970.

* Engineer, now a Student at Massachusetts Institute of Technology. Honorary Fellow AIAA.
† Project Engineer. Member AIAA.
‡ Research Physicist. Member AIAA.

1. Radar Observables

RANGE radar measurements of rocket launches have been made at various frequencies in the hf band and at various aspect angles. Generally radar backscatter from rocket plumes in this radar band exhibits a bimodal Doppler frequency spectrum which will depend on the aspect angle. For the purpose of this paper we have restricted our treatment to the tail aspect geometry shown in Fig. 1. One signal in the return spectrum is associated with the rocket vehicle and attached shock structure, which are relatively smooth surfaces moving at the vehicle velocity. This signal covers a narrow spectral region and is called the "enhanced skin echo." A second signal which may appear is called the "exhaust Doppler echo;" Doppler shifted from the "enhanced skin echo." It covers a broad spectral region. This signal appears to originate from a large collection of scatterers moving with a velocity distribution Doppler shifted from the vehicle velocity by approximately the exhaust limiting velocity ($\sim$3 km/sec). Thus these scatterers have been associated with the rocket exhaust. The exhaust Doppler return is here assumed to be the result of electromagnetic plane wave (radar) scattering from partially correlated ionized turbulence in the rocket exhaust.

The form of these radar returns observed by a CW Doppler radar operating at hf is shown in Fig. 2. This figure is an actual Doppler-time history of the radar return obtained

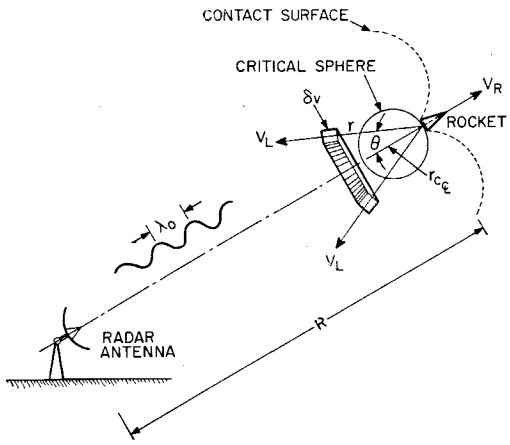

Fig. 1 Radar backscatter geometry at tail aspect angle.

during a typical rocket launch. The display was obtained using a "Rayspan" signal analyzer. The return is positioned along the ordinate as a function of Doppler shift from the radar carrier. These displays are generally intensity modulated so that the strength of the return is represented by the "grey scale" darkness of the record. However, the dynamic range of this scale is rather limited, generally on the order of 6 db or less, consequently, to obtain information concerning the relative strengths of these returns, other techniques must be used. Fig. 3 is a display of the relative amplitude of the Doppler returns using a "Vibralyzer" in its sectioning mode. However, in this type of display the Doppler spectrum of the return is shown only at a particular time of the flight for each display. In this particular case the spectrum was made at the time t_1 shown in Fig. 2.

For tailaspect geometry the enhanced skin return is at a frequency corresponding to return from a body moving at the rocket velocity V_R whereas the exhaust Doppler, spread over a much larger frequency range, is at a higher frequency generally. The location of the carrier is arbitrary and fixed and the return tends to move as a fixed bimodal pattern toward lower frequencies with respect to the carrier as the rocket accelerates along its trajectory. Observations have shown that the effect of the ionized exhaust flowfield becomes more prominent as the radar frequency is reduced. Radar return in the hf band (3–30 MHz) has significant contributions from this flowfield. The structure of the return in this band is considerably different from what it is at higher radar frequencies (0.3–3 kMHz). Further observations have shown that even at hf, the low-altitude return from the exhaust flow is considerably smaller than it is at high altitude (>100 km) where exhaust dimensions are on the order of kilometers and a large volume is occupied by an underdense and turbulent ionized fluid.

Booker and Gordon[1] originally developed an expression for the scattering of radio waves by dielectric turbulence from a volume of linear dimensions much larger than the turbulence scale. Silverman[2] and Tatarski[3] have criticized Booker and Gordon's result from the standpoint of the turbulence structure, Tatarski pointing out that when $(2\pi l/\lambda_0)\sin(\theta/2) \gg 1$, important errors can be anticipated. Guthart et al.,[4] measuring the microwave scattering of a plasmajet in the range $2\pi l/\lambda_0 \sim 1$, confirmed some aspects of the Booker-Gordon scattering expression for a highly nonuniform turbulent flow. Guthart et al. remark that the difference between the Booker and Gordon and the Komolgorov correlation functions was negligible in the context of their measurements.

One of the first applications of scattering from dielectric turbulence in the flow behind an aerodynamic vehicle was by Pippert,[5] who considered radar measurements of wake turbulence. An excellent theoretical analysis of backscattering from a weakly ionized turbulent wake is that of Lane.[6]

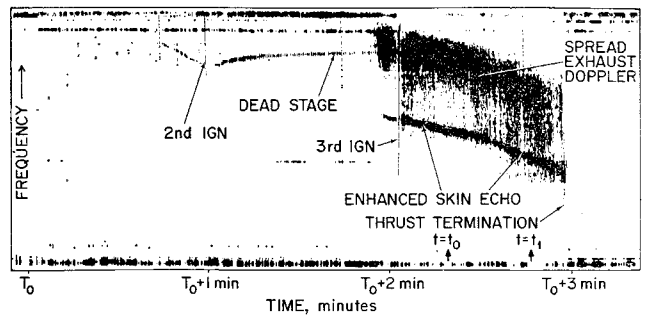

Fig. 2 Radar backscatter history of launch with return frequency vs time into trajectory.

He considered the frequency effects of the radar return for several wake turbulence models. Lane felt that the turbulence model was one of the weakest aspects of wake analysis at present, together with the resolution and sophistication of present signal processing techniques. No farfield rocket exhaust turbulence models have been either theoretically or experimentally studied. Again there is no available work, analogous to Lane's for the wake, that has been carried out for radar back scatter from rocket exhausts. The interaction of radio waves with rocket exhausts has been studied in connection with mean attenuation of microwaves propagating through the entire exhaust flow including the potential or vacuum core, the inner shock layer and the fuel rich (sometimes) mixing layer. Smoot and Underwood[7] carried out exhaust flow attenuation studies in the VHF and SHF (200 MHz–10 kMHz). However these frequencies are such that the high-altitude vacuum exhaust is neglected ($f_p \ll f_o$) and the fuel-rich afterburning mixing layer is of prime concern at lower altitudes[8] (<60 km).

In this paper an approximate analysis of the magnitude and spectral distribution of radar return from turbulent vacuum exhausts frozen downstream of the rocket nozzle is carried out. Lacking experimental studies of the exhaust turbulence, a simple model is proposed with the intention of expressing the physics of the flow and yet obtaining a simple expression for the radar cross section. The expressions obtained show the effect of nonuniform combustion, mean gas properties, and engine parameters on the radar return.

The principle assumptions made are:

1) The return is from the vacuum (potential) exhaust. For high-altitude (>100 km) vehicles return from the plume mixing layer can usually be neglected because of low densities.[8] Further, the large plume scale (~3 km) results in a large volume of vacuum exhaust flow. Secondary flows, e.g. multinozzle base flows[12] (caused by specific base geometries) or recirculation caused by flow separation at extreme altitudes,[13] are neglected.

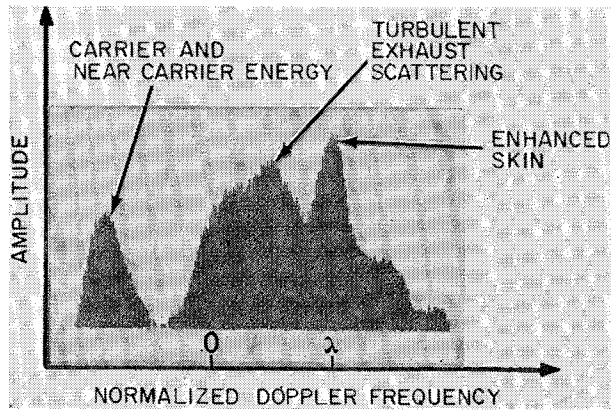

Fig. 3 Radar backscatter amplitude frequency spectrum at time into trajectory = t_1.

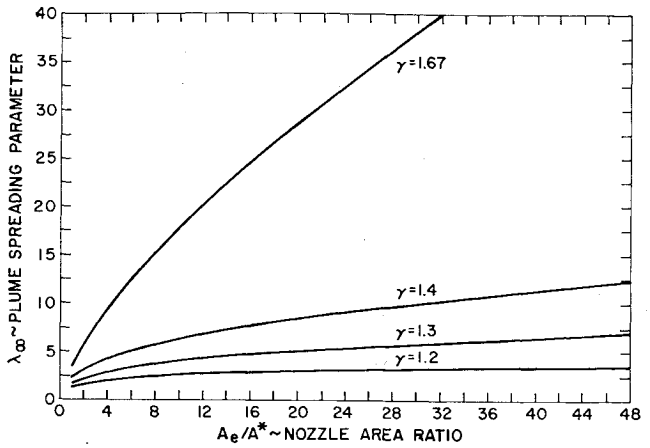

Fig. 4 Variation of plume spreading parameter with nozzle area ratio.

2) The vacuum exhaust mean flow is radial from the exit plane with mass distribution given by Eq. (1) and speed $\sim V_L$.

3) The electrons are frozen beyond the exit (which holds for certain exhausts[8]).

4a) The vacuum exhaust nonuniformities (e.g., entropy spottiness) originate solely in stagnation temperature nonuniformities.

b) The scattering eddy velocity distribution is gaussian. Whereas this velocity distribution may not apply to all eddy sizes, most scattering is caused by a limited range of eddy sizes (Bragg condition[3]).

c) Electron density is correlated with neutral particle density and kinetic temperature as in the far field the debye length to hf backscattering eddy scale ratio is small, where T and n are important. Since the debye length $\sim(T/n_e)^{1/2}$ for the far field exhaust it varies as $(T_{\text{exit}}/T)^{(2-\gamma)/2(\gamma-1)}$ and the above ratio is small for $T > 10°\text{K}$.

d) At V_L stagnation temperature perturbations do not perturb the local Mach number so that velocity perturbations will be taken to lie principally along local streamlines.

e) The isotropic exponential correlation function will, for simplicity, be used. In the hf, $\lambda_0 \sim 10\text{m}$, where $2\pi l/\lambda_0 \sim 1$, taking $l \sim d_e$ say, there is little difference between the exponential and Kolmogovov functions.[3] Moreover, "Crocco" turbulence $V \sim V_L$ has not been examined in depth warranting a more refined approach now.

f) Distortion of the turbulence by the geomagnetic field is ignored. Al'pert and Pitaevskii[9] and Rand and Albini[10] discuss the geomagnetic field effect on wake backscatter.

2. Turbulent Exhaust Scattering Model

The sources of the exhaust Doppler return are weakly ionized scattering eddies fluctuating parallel to the mean flow streamlines with a gaussian velocity distribution. The exhaust mean flow Sec. 2.1, turbulence Sec. 2.2, and radar scattering areas are considered below.

2.1 Farfield Rocket Exhaust Model

A simple and useful farfield (gas speed $\sim V_L$) exhaust model describing the mass flow $d\dot{m}$ through a solid angle $d\Omega$ centered on a ray inclined with angle θ relative to the exhaust centerline (see Fig. 1) will be used here[14]

$$(d\dot{m}/d\Omega)_\theta/(d\dot{m}/d\Omega)_{\theta=0} = \exp[-\lambda_\infty{}^2\eta^2] \qquad (1)$$

where $\lambda_\infty = [\pi^{1/2}(1 - C_F/C_{F\max})]^{-1}$. The farfield exhaust spreading parameter λ_∞ shown in Fig. 4, varies such that $\lambda(A_e/A^* \to \infty) \to \infty$ indicating all the mass flow is parallel to $\theta = 0$. This model has been used to estimate Mach disc locations in two-phase flow,[15] radiative profiles in liquid engine exhausts,[16] and exhaust rarefaction onset.[17] The approximation of Eq. (1) is suitable for use here. The restriction to the farfield flow model is not serious since for high-altitude plumes the flow in the vicinity of the exit represents a small fraction of the total scattering volume and this region is often within the overdense region ($f_p \gg f_o$). It will be useful to define the centerline decay parameter B in terms of the model of Eq. (1) for specification of the frozen electron density n within the plume

$$B \equiv \rho r^2/\rho_c d^{*2} = [2/(\gamma+1)]^{1/(\gamma-1)}[(\gamma-1)/(\gamma+1)]^{1/2}\lambda_\infty/4\pi^{1/2} \qquad (2)$$

2.2 Vacuum Exhaust Flow Turbulence

A model of the turbulence in a combustion generated radially expanding supersonic flow is not available. Here a simple nonisotropic turbulence model is suggested based on the assumptions of section 1.0.

The combustion chamber rms temperature fluctuation intensity $(\overline{\theta_c^2})^{1/2}/\bar{T}_c$ is assumed known and the effect of supersonic expansion on this fluctuation is required. Corrsin[18] has considered this problem by examining perturbations of known magnitude (subscript 1) in streamtube properties as the flow adiabatically expands downstream to unknown perturbation magnitudes (subscript 2). Assuming that the rms velocity turbulence intensities are small, $(\overline{u_1^2})^{1/2}/\bar{V}_1 \ll 1$ and $(\overline{u_2^2})^{1/2}/\bar{V}_2 \ll 1$, then

$$(\overline{u_2^2})^{1/2}/\bar{V}_2 = (\bar{M}_1/\bar{M}_2)^2(\overline{u_1^2})^{1/2}/\bar{V}_1 + [1 - (\bar{M}_1/\bar{M}_2)^2](\overline{\theta_c^2})^{1/2}/2\bar{T}_c \qquad (3)$$

and the temperature fluctuation intensity is unchanged. Assume the expansion is from $\bar{M}_1 \approx 0$ to $\bar{M}_2 \gg 1$ such that $\bar{V}_2 \sim \bar{V}_L$, then, in the farfield

$$(\overline{u^2})^{1/2}/\bar{V}_L = (\overline{\theta^2})^{1/2}/2\bar{T} = (\overline{\theta_c^2})^{1/2}/2\bar{T}_c \qquad (4)$$

Since pressure forces are negligible in the farfield, pressure turbulence will be ignored. Taking the electrons frozen, the dielectric turbulence is correlated with the velocity and temperature (entropy) fields ($dn/n = (\gamma-1)^{-1}dT/T$). This is a stronger condition than that of identical statistics used in the case of dielectric noise caused by turbulent mixing.[2]

Assuming that the velocity distribution of the perturbation u about the mean $\bar{V}_L$ is gaussian, then

$$P(V_L) = (2\pi\overline{u^2})^{-1/2}\exp[-(V_L - \bar{V}_L)^2/2\overline{u^2}] \qquad (5)$$

where $V_L = \bar{V}_L + u$ and

$$\int_{-\infty}^{+\infty} P(V_L)dV_L = 1$$

In Eq. (5), $\overline{u^2}$ applies to the scattering eddies and may depend on λ_0 but for the present $\overline{u^2}$ will be found using Eq. (4). Since both the limiting velocity and the local speed of sound vary as $(T_c)^{1/2}$, a perturbation in T_c will not perturb the local Mach number. This is to say that lateral disturbances do not propagate, longitudinal disturbances arise from changes in T_c, and the velocity fluctuations lie along local streamlines.

The turbulence properties of a highly expanded rocket exhaust are presently unknown. For many flows, however, above the viscous cut off the spectrum is approximately constant for small wave numbers, and then has an inertial subrange. One model of this behavior leads to correlation function of $K_{1/3}(s/l)$, which is approximately proportional to $(s/l)^{1/6}\exp(-s/l)$.

Since the one-sixth power dependence is weak, the turbulence will be described by an isotropic exponential correlation function $R = \exp(-s/l)$. The scale l will be assumed to be-

have as 1) a constant and 2) $\sim\alpha r$, where $\alpha \ll 1$ is a constant. The second case is prompted by the lateral expansion with r of the flow. The flow is not isotropic generally, but it may be "locally" isotropic over a distance smaller than that in which flow properties change significantly but larger than l. In this event $l \sim \alpha r$ may not be applicable.

2.3 Scattering from Dielectric Turbulence

Scattering expressions for underdense ($f_p \ll f_o$) turbulent plasmas have been derived giving the effective cross section for scattering per solid angle[3]

$$\sigma = 2\pi k^4 V \sin^2\chi\Phi[2k \sin(\phi/2)] \quad (6)$$

where χ is the angle between the illuminating field in the scattering volume and the vector from that volume to the receiver and ϕ is the scattering angle (usually θ) such that $\phi = 0$ corresponds to forward scattering. For $R = \exp(-s/l)$ there results the power spectrum $\Phi(2k \sin(\phi/2)) = \overline{n_1^2} l^3/\pi^2[1 + 4k^2l^2 \sin^2(\phi/2)]^2$ and the radar cross section becomes

$$\sigma_u = 4\pi\sigma = 8\pi\sigma_T l^3 \bar{n}^2 V(\overline{\delta n^2}/\bar{n}^2)(1 + 4k^2l^2)^{-2} \quad (7)$$

since $\chi = \pi/2$ and $\phi = \pi$ for backscattering and where $\overline{n_1^2} = \pi\sigma_T\, \overline{\delta n^2} k^{-4}$ is the mean square deviation of the index of refraction from the mean. The mean square electron fluctuation intensity $\overline{\delta n^2}/\bar{n}^2 = (\gamma - 1)^{-2}\overline{\theta^2}/\bar{T}^2$ is found using Eq. (5) and $\bar{n}$ is found using Eq. (2) as $\bar{n}/\bar{n}_c = \bar{\rho}/\bar{\rho}_c$.

Multiple scattering from the overdense region fluctuating boundary has been neglected. However, the surface fluction spectrum at this boundary will be closely related to the exhaust turbulence and the exhaust Doppler contribution from this surface is expected to have a form similar to that derived below for the underdense return.

3. Exhaust Doppler Cross Sections

The elements considered previously will be used to make an analytic estimate of the exhaust radar cross sections. The total cross section, neglecting the overdense region, is calculated in Sec. 3.1 and the exhaust Doppler spectrum is calculated in Sec. 3.2.

3.1 Total Radar Cross Sections

The turbulent scattering of Eq. (7) applies when the elemental volume δv linear dimensions are large compared to l. Here we take $\delta v = 2\pi r^2 \sin\theta d\theta dr$ (see Fig. 1). The receiver-plume distance is assumed very large so that the illuminating field vector is constant throughout the plume. The cross section of δv for $l = \alpha r$ becomes

$$\delta\sigma_u = A(4/\pi)^{1/2}(1 + r')^{-2} \exp[-\eta'^2]d\eta' dr' \quad (8)$$

when $\eta' = 2^{1/2}\lambda_\infty\eta$, $r' = 4k^2\alpha^2 r^2$, and

$$A = 3\pi^{-1/2}2^{-15/2}[2/(\gamma + 1)]^{2/(\gamma-1)}/(\gamma^2 - 1) \times \sigma_T\lambda_\infty n_c^2\alpha^3 d^{*6}(\lambda_0/d^*)^2(\overline{\delta n^2}/\bar{n}^2) \quad (9)$$

If $\delta\sigma_u$ is integrated over the entire plume volume the vacuum exhaust cross section σ_v for an entirely underdense ($f_p \ll f_o$) plume is obtained

$$\sigma_v = A\int_0^\infty \frac{dr'}{(1 + r')^2}\int_0^{2^{3/2}\lambda_\infty} \frac{2\exp(-\eta'^2)d\eta')}{\pi^{1/2}} = A \quad (10)$$

For most high-altitude engines (e.g., $A_e/A^* = 25$, $\gamma = 1.2)\lambda_\infty > 2$, and $erf(2^{3/2}\lambda_\infty) \sim 1.0$.

There often exists an overdense region ($f_p > f_o$) near the exit with a downstream boundary at r_c where the electron density n_o is such that $f_p = f_o$. From the model of Eq. (1)

$$r_c' = 4k^2\alpha^2 r_c^2 = 4\pi^{3/2}[2/(\gamma + 1)^{1/(\gamma-1)} \times [(\gamma - 1)/(\gamma + 1)]^{1/2}\lambda_\infty(n_c/n_o)(\alpha d^*/\lambda_0)^2 \times \exp(-\eta'^2/2) = R_o \exp(-\eta'^2/2) \quad (11)$$

where R_o is the centerline ($\theta = 0$)r_c' value. The underdense exhaust cross section σ_u results

$$\frac{\sigma_u}{\sigma_v} = \int_0^{2^{3/2}\lambda_\infty} \frac{2\exp[-\eta'^2]d\eta'}{\pi^{1/2}}\int_{1+r_c'}^\infty \frac{dr'}{r'^2} \cong \frac{2^{3/2}}{\pi^{1/2}}\int_0^\infty \frac{e^{-x^2}dx}{e^{x^2} + R_o} \quad (12)$$

The ratios σ_u/σ_v for $l = \alpha r$ and $l =$ constant are shown in Fig. 5. For $l = \alpha r$ if the l for maximum return Eq. (7) lies outside r_c (r_c small), then r_c has little effect on σ_u/σ_v. If this l lies inside the overdense region the return σ_u/σ_v rapidly falls with increasing r_c because of decreasing electron densities and increasing l. For $l =$ constant σ_u/σ_v falls less rapidly solely due to decreasing electron densities. Certainly exhaust turbulence studies should include simultaneous measurements at several frequencies. In any event, the absolute cross section for a given vehicle can vary significantly (e.g., from day to night shots) whereas the exhaust Doppler spectrum is more constant.

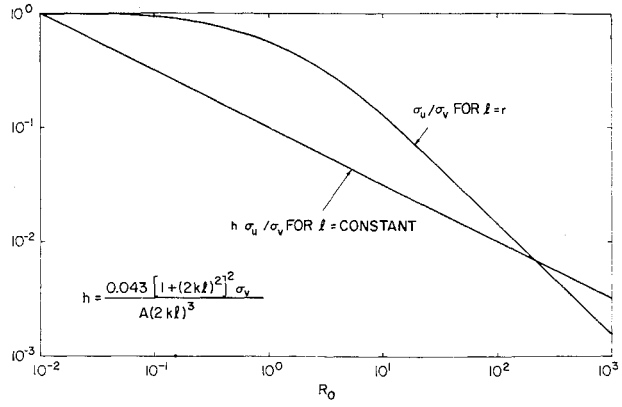

Fig. 5 Exhaust Doppler radar cross section for two turbulence models.

3.2 Exhaust Doppler Spectrum

The exhaust Doppler spectrum is first derived for the mean flow $\bar{u}^2 = 0$ which is then considered redistributed by the velocity fluctuations, $\overline{u^2} \neq 0$, where the instantaneous velocity is $V_L = \bar{V}_L + u$. A volume element on a radial streamline at angle θ to the exhaust centerline illuminated with frequency f_o will return the signal at f

$$f = f_o\{1 + 2[V_L(1 - \eta) - V_R]/c\} \quad (13)$$

where V_R is the rocket speed and V_L changes negligibly over many cycles of f_o. The mean flow $u = 0$ in a hollow cone from η to $\eta + d\eta$ contributes the return $d\sigma_u$

$$d\sigma_u = \sigma_v 2\pi^{-1/2}\exp[-\eta'^2](1 + r_o' \exp[+\eta'^2/2])^{-1}d\eta' \quad (14)$$

centered at $f_c = f_o\{1 + 2[\bar{V}_L(1 - \eta) - V_R]/c\}$. This frequency changes with angle as

$$df_c = -2f_o(\bar{V}_L/c\lambda_\infty)d\eta = Dd\eta \quad (15)$$

such that

$$d\sigma_u/df_c = \sigma_v 2^{3/2}\exp(-\lambda_\infty^2\eta^2)\{D\pi^{1/2}[\exp(\lambda_\infty^2\eta^2) + R_o]\}^{-1} \quad (16)$$

Defining $f_{max} = f_o[1 + 2(\bar{V}_L - V_R)/c]$ and the exhaust

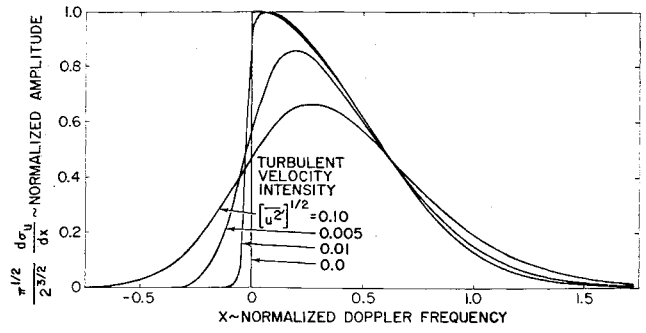

Fig. 6 Variation of normalized Doppler spectra with turbulent intensity.

Doppler spectrum in terms of a nondimensional center frequency $x_c = \lambda_\infty \eta = (f_c - f_{max})/D$, the mean return per frequency interval is

$$d\sigma_u/dx_c = \sigma_v 2^{3/2}\pi \exp[-x_c^2][\exp(x_c^2) + R_o]^{-1} \quad (17)$$

This mean flow exhaust Doppler is shown in Fig. 6 for $R_o = 0$ by the curve labeled $[\overline{u^{2\prime}}]^{1/2} = 0$. As real frequency increases for decreasing x_c, there is a sharp cut-off corresponding to return from flow moving at V_L directly toward the receiver ($\theta = 0$) and a tail caused by the return from laterally moving fluid $\theta \neq 0$. Use of the normalized amplitude results in a turbulent cross section which is actually nonexistent for $\overline{u^2} = 0$.

We make the approximation that the mean Doppler spectrum is redistributed by the velocity fluctuations. Taking $u' = u/\bar{V}_L$, then u' is expressed in terms of x as $u' = (x_c - x)/(x_c + \lambda_\infty)$ where $x = (f - f_{max})/D$. The contribution to the return $d\sigma_u$ from the center frequency x_c to the frequency range x, $x + dx$ is

$$d\sigma_u/dx = 2(\pi\overline{u^{\prime 2}})^{-1/2}\sigma_v \exp(-x_c^2)[\exp(x_c^2) + R_o]^{-1} \times \exp\{-(1/2\overline{u^{\prime 2}})[(x_c - x)/(x_c + \lambda_\infty)]^2\} d(x_c - x)/(x_c + \lambda_\infty) \quad (18)$$

The contribution to x from all x_c is found by integrating $\tau = x_c - x$ over $-x < \tau < +\infty$

$$d\sigma_u/dx = 2(\pi\overline{u^{\prime 2}})^{-1/2}\sigma_v \times \int_{-x}^{\infty} \frac{\exp\{-(1/2\overline{u^{\prime 2}})[-\tau/(x + \tau + \lambda_\infty)]^2\}(x + \lambda_\infty)d\tau}{(x + \tau + \lambda_\infty)^2 \exp[(x + \tau)^2]\{\exp[(x + \tau)^2] + R_o'\}} \quad (19)$$

The exhaust Doppler cross section is shown in Fig. 6 for $(\overline{u^{\prime 2}})^{1/2} = 0.01$, 0.05, 0.10 together with the mean exhaust Doppler. The turbulence smooths out the high-frequency edge ($f = f_{max}$), shifts the peak toward the mean exhaust Doppler spectrum centroid, but negligibly affects the low-frequency tail. For $\overline{u^2}$ large the spectrum becomes gaussian.

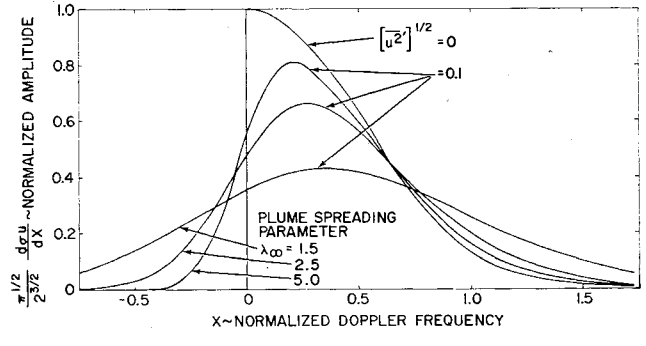

Fig. 7 Variation of normalized Doppler spectra with plume spreading parameter.

The effect of engine design is shown in Fig. 7 by varying λ_∞ for $(\overline{u^{\prime 2}})^{1/2} = 0.10$. By increasing γ or A_e/A^* (i.e., reducing the available internal energy for exhaust expansion beyond the exit) λ_∞ increases leading to more of the mass flow near $\theta = 0$ and thus narrowing the exhaust Doppler spectrum. From the engine parameters ($\lambda_\infty = 2.8$) of the vehicle shown in Fig. 2 the respective positions of the enhanced skin and exhaust Doppler are shown in Fig. 8 for time $t = t_o$ (the relative amplitudes are arbitrary). A great deal of difficulty was experienced in obtaining spectra (e.g., Fig. 3) from the data of Fig. 2 because of the lack of equipment for signal processing these data. Ideally several spectra should be taken from Fig. 2 but the authors were able to obtain only $t = t_1$. This spectrum shows significant energy around the enhanced skin (occurring at the higher altitudes of Fig. 2) which may be scattering off secondary flows in the vicinity of the vehicle that develop at higher altitudes. At lower altitudes there is the possibility of significant contributions from a reacting mixing layer and in general we would not expect to see the exhaust Doppler spectrum alone. However, for a large portion of the lower altitude section of Fig. 2 the exhaust Doppler and enhanced skin returns are well separated and constant in form. The exhaust Doppler spectrum shows a relatively sharp high-frequency edge with a more gradual low-frequency tail toward the enhanced skin as ideally expected. The boundaries of the exhaust Doppler spectrum region from Fig. 2 are plotted on Fig. 8 with respect to the enhanced skin. The Doppler return spectra (Fig. 6) are modified for large fluctuation intensities because of the assumed electron density—eddy speed correlation. When the Doppler spectrum at larger fluctuation intensities is approximated by a gaussian function which is weighted by the increase in mean square electron density with gas speed Eq. (4), there results a gain of total Doppler cross section of $\sim 4\overline{u^{\prime 2}}/(\gamma - 1)^2$ db and a stretching of the Doppler spectrum away from the enhanced skin by $(1 + 4\overline{u^{\prime 2}}/(\gamma - 1))(x - \lambda_\infty)$. These factors become important as $(\overline{u^{\prime 2}})^{1/2} \to 0.1$ for $\gamma = 1.2$ but then the local temperature perturbations are no longer small.

4. Discussion

The present approximation has demonstrated the main features of the observed exhaust Doppler return spectrum; the detached spectrum, its shape, and location. It would be valuable to analyze the other possible sources of radar return that is frequency shifted from the enhanced skin. The plume mixing layer at lower altitudes and internozzle (i.e., base) flow and recirculation due to jet pluming at higher altitudes might be such sources. These latter contributions would vary with altitude whereas the exhaust Doppler return is constant with altitude. Reflection from the overdense region would be independent of altitude and likely of a form

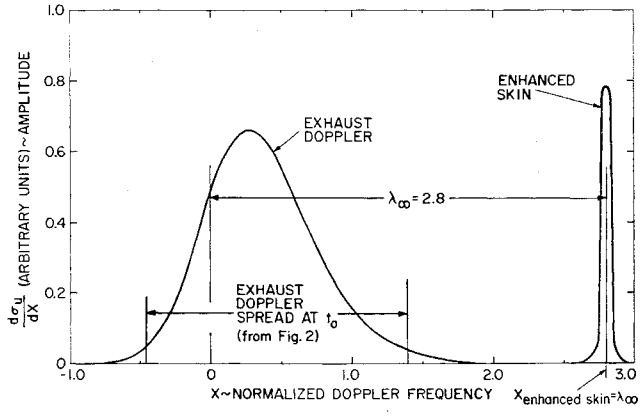

Fig. 8 Theoretical radar return spectra.

similar to the underdense return. Analysis of this reflection would be useful to determine its magnitude relative to the underdense return.

The exhaust turbulence model has been kept as simple as possible but suggests the large scale ($kl \sim 1$) anisotropic nonuniformities to be expected in the farfield exhaust. The nature of the farfield exhaust turbulence can certainly be studied by radar. For example, the parameter u^2 describing the scattering eddy fluctuations can be surveyed by measurement of the high-frequency band edge as a function of radar frequency. Improvement of the turbulence model and the related signal processing techniques is certainly in order. Ultimately, radar techniques could be developed to monitor engine operation outside the atmosphere.

In light of the approximation discussed here it is interesting to make a comparison with Lane's[6] results for the wake radar return. Lane considered the frequency effects in range gated return from wakes at a 45° aspect angle. Range gating provided Lane with a single mean defect velocity hodograph. For zero velocity fluctuation ($K = 0$)[6] this leads to the mean return spectrum caused by nonuniformity in mean velocity with a sharp cutoff at the maximum defect velocity shifted in frequency from the vehicle return. For nonzero velocity fluctuations ($K = 0.05, 0.10$)[6] the return spectrum spreads rapidly from the relatively narrow mean wake spectrum. These effects are shown by Lane as cases C_1, C_2, and D in Fig. 9 which is analogous to Fig. 6 of this paper (excepting the amplitude normalization). Lane's nondimensionalized frequency μ_m is related by constants to the normalized frequency x used here. Since the entire farfield exhaust is specified by one circle in the hodograph plane its cw return is analogous to Lane's range gated wake spectra. As the exhaust return is usually much better separated from the vehicle echo than is the wake return, study of launch vehicle backscatter should be very useful and present understanding of the connection between backscatter and engine design waits on such studies.

References

[1] Booker, H. G. and Gordon, W. E., "A Theory of Radio Scattering in the Troposphere," *Proceedings of the IRE*, Vol. 38, No. 401, 1950.

[2] Silverman, R. A., "Fading of Radio Waves by Dielectric Turbulence," *Journal of Applied Physics*, Vol. 28, No. 4, April 1957.

[3] Tatarski, V. I., *Wave Propagation in a Turbulent Medium*, McGraw-Hill, New York, 1961.

[4] Guthart, H., Weissman, D. E., and Morita, T., "Diagnostics and Microwave Scattering for an Underdense Turbulent Plasma," TR 27, May 1965, Stanford Research Institute.

[5] Pippert, G. F., "On the Structure of Wake Turbulence Deduced from Field Radar Measurements," AIAA Paper 63-446, Cambridge, Mass., 1963.

[6] Lane, F., "Frequency Effects in the Radar Return from Turbulent Weakly Ionized Missile Wakes," *AIAA Journal*, Vol. 5, No. 12, Dec. 1967.

[7] Smoot, L. D. and Underwood, D. L., "Prediction of Microwave Attenuation Characteristics of Rocket Exhausts," *Journal of Spacecraft*, Vol. 3, No. 3, March 1966.

[8] Ely, O. P. and Hockenberger, R. W., "Rocket Exhaust Effects on Radio Frequency Transmission," *Journal of Spacecraft*, Vol. 3, No. 3, March 1966.

[9] Al'pert, Y. L. and Pitaevskii, L. P., "Scattering of Electromagnetic Waves by Inhomogeneities Excited in a Plasma by a Rapidly Moving Body," *AIAA Journal*, Vol. 1, No. 4, April 1963.

[10] Rand, S. and Albini, F., "Radar Return from Vehicles in the Ionosphere," *AIAA Journal*, Vol. 5, No. 6, June 1967.

[11] Batchelor, G. K., *The Theory of Homogeneous Turbulence*, Cambridge Univ. Press, Cambridge, Mass., 1963.

[12] Goethert, B. H., "Base Flow Characteristics of Missiles with Cluster-Rocket Exhausts," *Aerospace Engineering*, Vol. 20, March 1961.

[13] Alpinieri, L. J. and Adams, R. H., "Flow Separation Due to Jet Pluming," *AIAA Journal*, Vol. 4, No. 10, April 1966.

[14] Hill, J. A. F. and Draper, J. S., "Analytical Approximation for the Flow from a Nozzle into a Vacuum," *Journal of Spacecraft*, Vol. 3, No. 10, Oct. 1966.

[15] Jarvinen, P. O. and Draper, J. S., "Underexpanded Gas-Particle Jets," *AIAA Journal*, Vol. 5, No. 4, April 1967.

[16] Rowe, J. D., White, H. M., and Gilbert, R. B., "Plume Spectral Analysis," *Rocket Plume Phenomena Specialists Meeting*, Aerospace Corp., El Segundo, Calif., July 1968.

[17] Draper, J. S. and Hill, J. A. F., "Rarefaction in Underexpanded Flows," *AIAA Journal*, Vol. 7, No. 7, July 1969.

[18] Corrsin, S., "Effect of Wind Tunnel Nozzle on Steady-Flow Non-Uniformities," *Journal of the Aeronautical Sciences*, Vol. 19, No. 2, Feb. 1952.